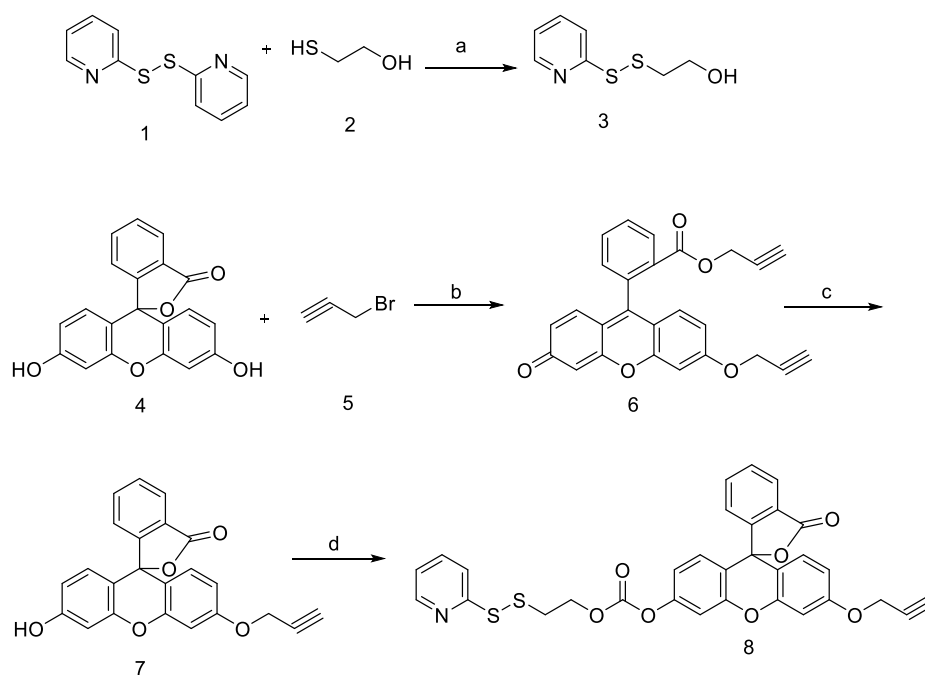# DNA nanodevices map enzymatic activity in organelles

Krishna Dan, Aneesh T. Veetil, Kasturi Chakraborty, Yamuna Krishnan*

E-mail: yamuna@uchicago.edu

Supplementary Scheme 1. Synthesis of thiopyridyl conjugated caged 6'-O propargyl fluorescein. Reagents and conditions: a) MeOH, rt, 12 h, yield = 72%, b) K_2CO_3, DMF, 65°C, 4 h. yield = 92%, c) NaOH, THF-H_2O, rt, 2 h. yield = 41%, d) Compound **3**, $COCl_2$, Et_3N, THF, yield = 40%

Synthesis of Compound **3**: The synthesis of compound **3** was partially followed from literature reported procedure[1]. 1 g (4.5 mmol) Aldrithiol was dissolved in 10 ml of methanol in a round bottom flask. 2-mercapto ethanol (0.106 ml, 1.5 mmol) was added dropwise and the reaction mixture was stirred overnight at room temperature for 12 h. Methanol was evaporated from the reaction mixture and the residue was purified by silica gel column chromatography using 30% ethyl-acetate in hexane as an eluent. Pure compound **3** was obtained as a colourless liquid in 72% yield. ^{1}H NMR (500MHz, $CDCl_3$, TMS): δ (ppm): 8.51 (m, 1H), 7.58 (m, 1H), 7.40 (m, 1H), 7.16 (m, 1H), 3.80 (t, 2H), 3.0 (t, 2H). HRMS: m/z calculated for $C_7H_9NOS_2$ = 187.0126, found 187.0128.

Synthesis of Compound **6**: Synthesis of compound **6** was modified from literature[2]. 1 g (2.5 mmol) Fluorescein was dissolved in 15 mL anhydrous DMF in a round bottom flask. 1.22 g

(10 mmol) anhydrous potassium carbonate followed by 0.82 ml propargyl bromide (10 mmol) was added to it. The reaction mixture was then stirred at 65°C for 4 h under inert atmosphere. DMF was evaporated under reduced pressure from the reaction mixture. The residue obtained was washed with water and filtered to afford a yellow solid as the product in 92% yield. ^{1}H NMR (500MHz, CDCl$_3$, TMS): δ (ppm): 8.25 (d, 1H), 7.80 (t, 1H), 7.68 (t, 1H), 7.33 (t, 1H), 7.06 (d, 1H), 6.81-6.79 (m, 3H), 6.55 (m, 1H), 6.45 (s, 1H), 4.79 (d, 2H), 4.58 (d, 2H), 2.61 (s, 1H), 2.33 (s, 1H). HRMS: m/z calculated for $C_{26}H_{16}O_5$ = 408.0998, found 408.0990.

Synthesis of Compound **7**: 0.8 g (1.9 mmol) compound **6** was dissolved in 5 mL THF in a round bottom flask. 2.5 g (62.5 mmol) NaOH was dissolved in 5 mL water and dropwise added to the reaction mixture. The mixture was stirred at room temperature for 4 h and THF was evaporated under reduced pressure. The pH of the reaction mixture was adjusted to 2 by adding concentrated hydrochloric acid dropwise. A yellow precipitate was collected by vacuum filtration. Further the precipitate was purified by silica gel column chromatography using 20% ethyl acetate in petroleum ether. Yield = 41%, ^{1}H NMR (500MHz, CDCl$_3$, TMS): δ (ppm): 8.02 (m, 1H), 7.67-7.63 (m, 2H), 7.17 (d, 1H), 6.87 (d, 1H), 6.74-6.69 (m, 4H), 6.54 (m, 1H), 4.72 (s, 2H), 2.56 (s, 1H), HRMS: m/z calculated for $C_{23}H_{14}O_5$ = 370.0841, found = 370.0848.

Synthesis of Compound **8** : Preparation of compound **8** was modified from the literature[3]. 126 mg (0.68 mmol) compound **3** was taken in a round bottom flask and 1 mL anhydrous THF was added to it under inert atmosphere. Then 4 mL (15 wt% in toluene) phosgene solution (CAUTION!) was added dropwise to the reaction mixture at 0°C and the mixture was stirred for 4 h. THF as well as phosgene was evaporated by purging N$_2$ through the reaction mixture in a fume hood to obtain corresponding chloroformate. This precipitate was dissolved in dry THF (1 mL) and kept under N$_2$ atmosphere. In a separate round bottom flask 50 mg of compound **7** (0.135 mmol), dissolved in 0.5 ml anhydrous THF and 0.115 mL (0.811 mmol) triethylamine was mixed and cooled to 0°C. The chloroformate containing THF was then added slowly over a period of 15 min to compound **7** containing reaction mixture and stirred at 0°C - RT overnight. After the completion, THF was evaporated from the reaction mixture under reduced pressure. Pure compound **8** was obtained by using preparative TLC (40% ethyl-acetate in hexane). Yield = 40%. ^{1}H NMR (500MHz, CDCl$_3$, TMS): δ (ppm): 8.45 (m, 1H), 8.03 (d, 1H), 7.63 (m, 5H), 7.17 (m, 1H), 7.11 (m, 2H), 6.88 (m, 1H), 6.82 (m, 1H), 6.72 (m, 2H), 4.72 (s, 2H), 4.52 (m, 2H), 3.14 (m, 2H), 2.56 (s, 1H). ^{13}C NMR (CDCl$_3$): δ (ppm): 169.1, 159.3, 152.9, 152.7, 152.1, 152.0, 151.9, 151.8, 149.8, 137.0, 135.1, 129.9, 129.1, 129.1, 129.1, 126.4, 125.1, 123.9, 121.0, 120.3, 120.1, 116.8, 112.5, 111.8, 109.7, 102.1, 82.1, 75.5, 66.4, 56.0, 36.8. HRMS: m/z calculated for $C_{31}H_{21}NO_7S_2$ = 583.076, found = 583.0759.

1
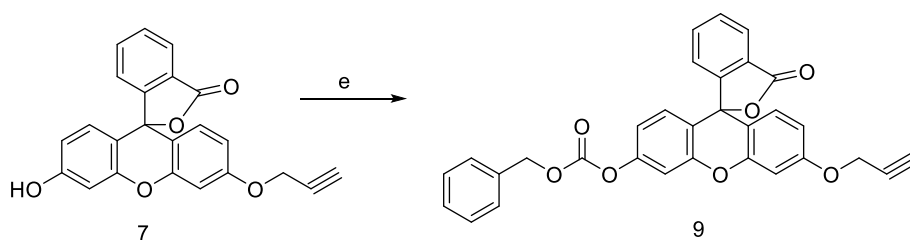
Supplementary Scheme 2: Synthesis of benzyl conjugated caged 6'-O propargyl fluorescein. Reagents and conditions: e) Benzyl chloride, Triethylamine, anhydrous THF, 0°C-rt, 12 h. yield = 80%

2 Synthesis of Compound **9**: 26 mg (0.07 mmol) compound **7** was dissolved in 2 mL anhydrous
3 THF. Then 98 µL (0.7 mmol) of triethylamine was added to it and stirred at 0°C under inert
4 atmosphere for 5 min. 50µL benzyl-chloroformate in 1 mL anhydrous THF was added
5 dropwise to the reaction mixture. The mixture was stirred at 0°C to room temperature under
6 inert atmosphere for 12 h. THF was evaporated under reduced pressure. The residue was
7 purified by silica gel flash column chromatography using 10% ethyl acetate in petroleum ether.
8 An off white solid was obtained as the product in 80% yield. ^{1}H NMR (500MHz, CDCl$_3$, TMS):
9 δ (ppm): 8.12 (d, 1H), 7.67 (m, 1H), 7.45 - 7.17 (m, 9H), 6.88 - 6.70 (m, 4H), 5.28 (s, 2H), 4.73
10 (d, 2H), 3.65 (s, 1H). ^{13}C NMR (CDCl$_3$): δ (ppm): 169.1, 159.3, 153.0, 152.9, 152.3, 152.2,
11 151.8, 151.5, 135.1, 134.4, 129.9, 128.7, 128.7, 128.6, 128.6, 127.5, 126.9, 126.1, 125.1,
12 123.9, 116.9, 116.8, 112.5, 111.8, 109.8, 102.1, 82.1, 76.0, 70.6, 65.4, 56.0. HRMS: m/z
13 calculated for $C_{31}H_{20}O_7$ = 504.1209, found = 504.1212.
14
15

1
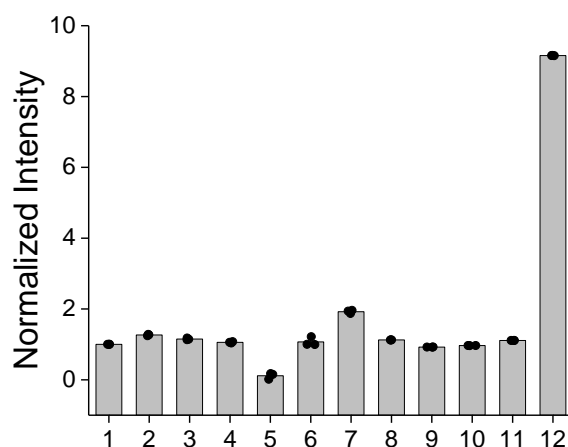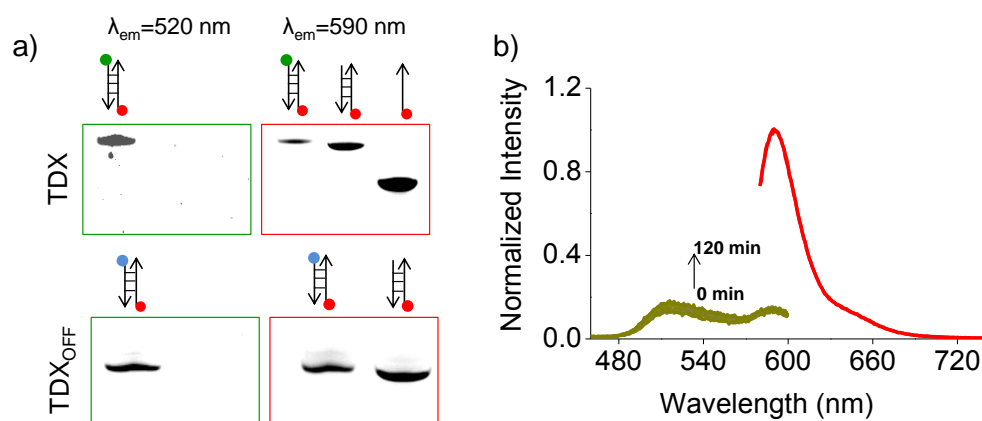
2
3
4 Supplementary Fig.1. a) 20 wt% native polyacrylamide gel electrophoresis of TDX reporter

5 (upper panel) and TDX_{OFF} reporter (lower panel). The gel was run for 3 h at 150 mV in

6 presence of 1X TBE (Tris-Borate-EDTA) buffer. b) Fluorescence signal evolution of TDX_{OFF} at

7 λ_{em} = 520 nm (green) and λ_{em} = 590 nm (red) in presence of 5 mM GSH at pH 7.2 at different

8 time point. c) Sensitivity of sensing dye, (compound **8**) in presence of different analyte such

9 as 1. Phosphate buffer (pH=7.2) and 1mM of 2. Na^+, 3. K^+, 4. Ca^{2+}, 5. Fe^{2+}, 6. Zn^{2+}, and 5 mM

10 of 7. H_2O_2, 8. His, 9. Ser, 10. Lys, 11. Val, and 12. Cys. Each intensity is normalized from the

11 intensity of compound **8** before treatment with respective analytes. Error bar indicates the

12 mean of three independent experiments ± s.e.m.

13

14

15
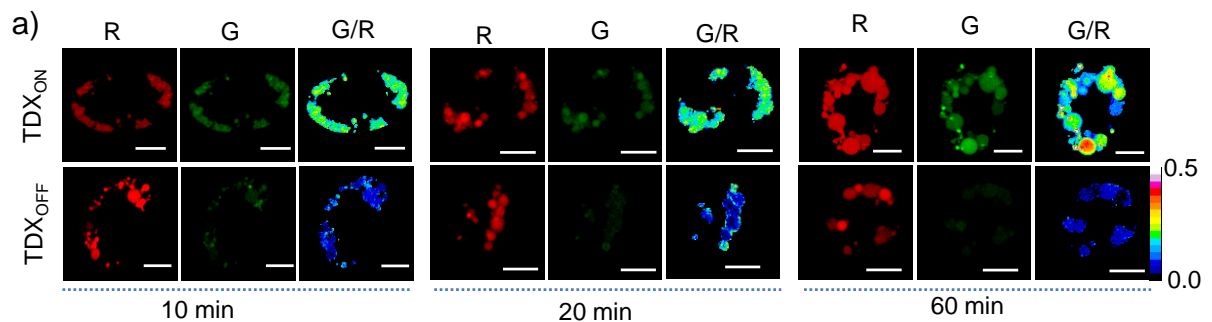
Supplementary Fig.2. a) Pseudocolour images of TDX$_{ON}$, (upper panel) and TDX$_{OFF}$ (lower panel) at 10 min, 20 min and 60 min post injection of wild type worm (N2). (n = 10 cells, ≥ 50 endosomes) Sale bar, 5μm.

Endosomal disulphide reduction is protein-mediated:

The observed intra-endosomal disulfide exchange could be mediated by small molecules like cysteine, glutathione, H$_2$S etc., or by enzymes [4–7]. To check which of these two scenarios is operational in endosomes of *C. elegans* we used a well-characterized, porous icosahedral DNA nanocapsule developed by our lab, which has a uniform pore size of 2.8 nm[8]. We created a chemically modified dextran (FD) bearing 2-3 disulphide sensing modules on average, the synthesis and characterization of which is presented in detail above (see in Supplementary page 5-6 and Supplementary Fig. 3). We then encapsulated the FD inside a DNA icosahedron bearing an Atto 647N label on one of the component strands to give I$^{A647}_{FD}$ (Supplementary Fig. 4a). The Atto 647N dye acts as a normalizing fluorophore as its fluorescence intensity at 665 nm (R) is independent of disulphide exchange while simultaneously functioning as a fiducial fluorophore to locate icosahedron inside coelomocytes. The synthesis and characterization for I$^{A647}_{FD}$ is also presented in the supporting information (Supplementary Fig. 3a).

Due to its well-defined, pore size I$^{A647}_{FD}$ should permit small thiols such as GSH, Cysteine, H$_2$S with size < 1 nm to pass freely through the capsule, access the chemically modified dextran FD encapsulated within and mediate disulphide exchange on FD. However, macromolecular thiols with sizes greater than 3 nm should not be able to access the interior of the icosahedron and therefore be unable to reduce the encapsulated FD. We tested I$^{A647}_{FD}$ for size selectivity towards disulphide exchange with a spectrum of differently sized thiols *in vitro* and observed that an increase in fluorescence intensity at 520 nm, (G) occurred only in the case of smaller size thiols such as glutathione, cysteine and H$_2$S, while larger thiols of

5

molecular weight > 10 kDa could not reduce FD (Supplementary Fig. 3b). The fold change in G/R ratio of I^{A647}_{FD} for complete disulphide exchange for this size selective reporter was found to be 9.4 (Supplementary Fig. 4b). We also made a sample of DNA icosahedron, carrying an Atto 647N label, and encapsulating FD which had been completely disulphide exchanged to give I^{A647}_{FD-ON}. We also made a sample of empty DNA icosahedron, carrying an Atto 647N label, without cargo inside to give I^{A647}_{FD-OFF}, to evaluate the contribution of autofluorescence.

We then used a tripartite nanocapsule reporter system comprising I^{A647}_{FD}, I^{A647}_{FD-OFF} and I^{A647}_{FD-ON} to test whether the observed intra-endosomal disulphide exchange was mediated by proteins or by small molecule thiols. Since DNA nanocapsules are also uptakes by scavenger receptors in coelomocytes, we injected either $I^{A647}_{FD,}$ I^{A647}_{FD-ON} or I^{A647}_{FD-OFF} into the pseudocoelom of N2 nematodes and acquired images in the fluorescein and Atto 647N channels at t = 30 min. If I^{A647}_{FD} undergoes disulphide reduction by small molecule thiols, then, it should show a G/R ratio like I^{A647}_{FD-ON}. Importantly, the G/R ratio of I^{A647}_{FD} at t = 30 min was only ~16% that of I^{A647}_{FD-ON} (Supplementary Fig. 4c and 4d). The resistance of I^{A647}_{FD} to turn on compared to TDX reveals that disulphide exchange due to small molecule thiols is insignificant within endosomes. In addition, a comparison of the *in vitro* and *in vivo* kinetics of disulphide exchange at pH = 6 strongly indicates that intra-endosomal disulphide exchange is enzyme catalysed (Fig. 1d and Fig. 2c).
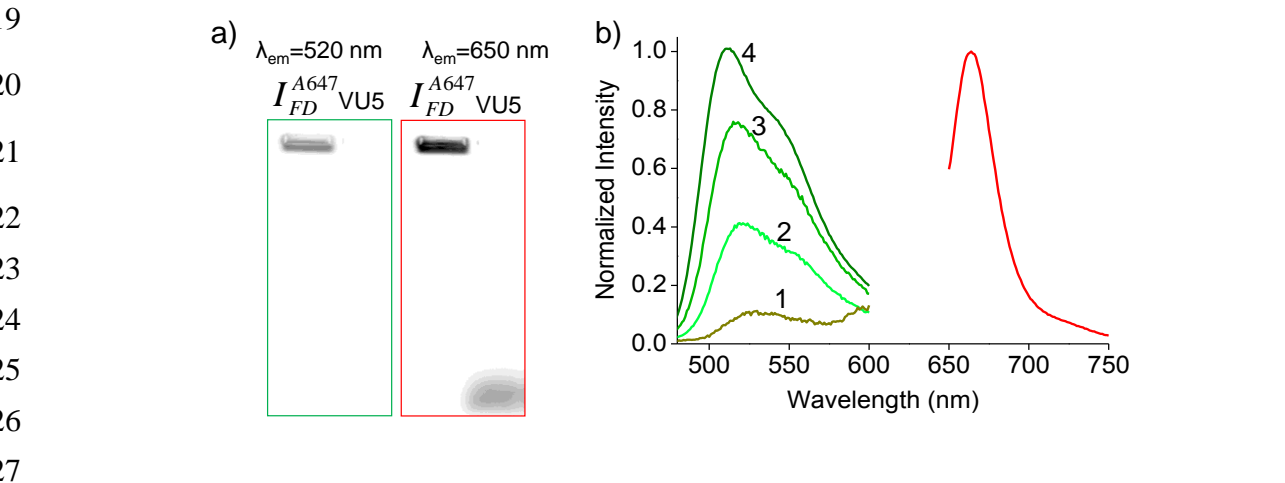
Supplementary Fig.3. a) 0.8 wt% Agarose gel electrophoresis of I^{A647}_{FD} (1st lane) and precursor of icosahedron VU$_5$ (2nd lane). The gel was run for 1 h at 100 mV in presence of 1X TAE (Tris base-acetic acid-EDTA) buffer. The gel was imaged in two channel at λ_{em} = 520 nm (green border) and λ_{em} = 660 nm (red border). b) Fluorescence signal evolution of I^{A647}_{FD} (3 μM) at λ_{em} = 520 nm (green) and λ_{em} = 660 nm (red) in presence of only buffer,(1) Dex-SH (trace 2, 40 kDa, 1 mM), Glutathione (trace 3, 1 mM) and H$_2$S (trace 4, 1 mM) in 0.1M phosphate buffer at pH = 7.2 at 1 h time point of incubation. In presence of smaller size thiol

1 such as glutathione and H$_2$S, I$^{A647}_{FD}$ shows increase emission at 520 nm wavelength compare

2 to that of bigger size thiols like Dextran-SH (40 kDa).

3

4
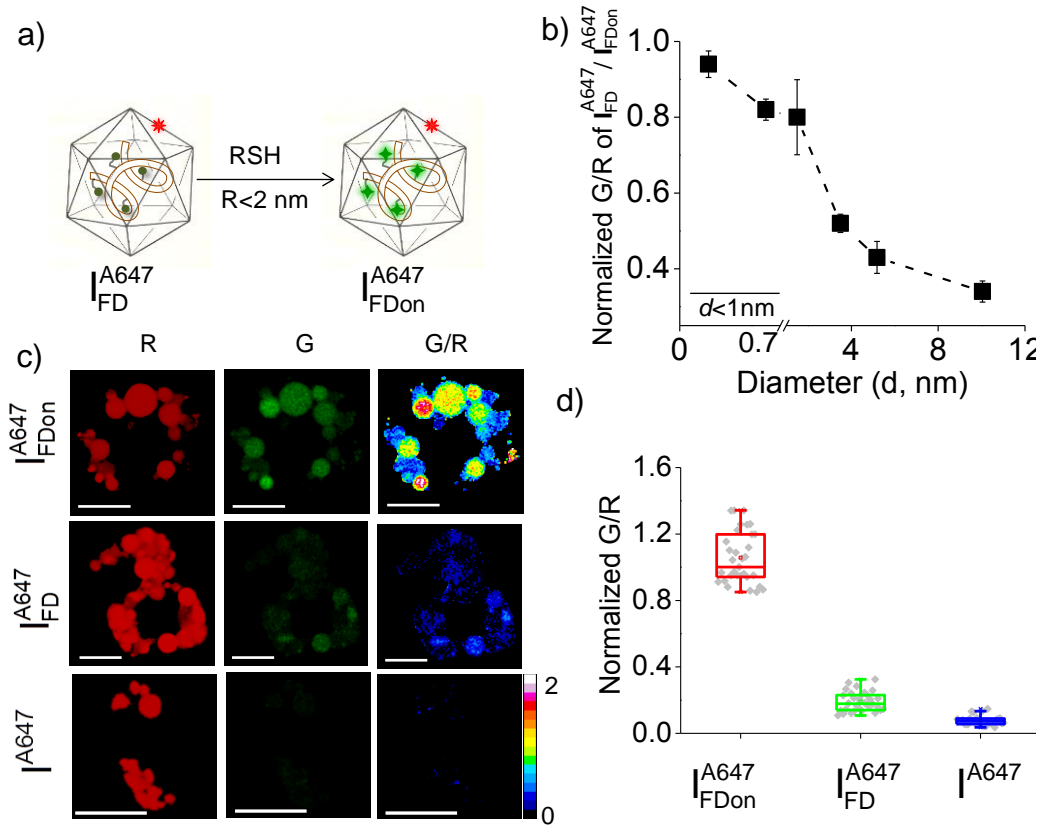
5 Supplementary Fig. 4. a) Pictorial representation of Atto 647N (red, R, λ_{em} = 670 nm) labeled

6 icosahedron containing chemically modified dextran conjugated to thiol sensing dyes (FD)

7 (green, G, λ_{em} = 520 nm) encapsulated inside it (left). I$^{A647}_{FD}$ undergoes disulfide exchange

8 reaction specifically with thiol which is less than 2 nm in diameter to form I$^{A647}_{FDon}$. b) Plot of

9 normalized G/R of I$^{A647}_{FD}$ over I$^{A647}_{FDon}$ after 1 h in presence of thiols of different sizes. The

10 thiols taken into consideration (from left to right) are H$_2$S (d = 0.2 nm), Cysteine (d = 0.6 nm),

11 GSH (d=1.5 nm), PEG-SH (3 kDa, d = 3.5 nm), Dex-SH (10 kDa, d = 5.2 nm) and Dex-SH (40

12 kDa, d = 10 nm). (Observed fluorescence intensity is G/R of I$^{A647}_{FD}$ / G/R of I$^{A647}_{FDon}$. c)

13 Representative pseudocolour images of I$^{A647}_{FDon}$ (upper panel), I$^{A647}_{FD}$ (middle panel), and

14 I^{A647}(lower panel) injected in the pseudocoelom of wild type worm and imaged 20 min post

15 injection, d) Plot of G/R ratio of I$^{A647}_{FDon,}$ I$^{A647}_{FD}$, I^{A647} from icosahedron labeled coelomocytes,

16 20 min post injection (n=10 cells, ≥ 50 endosomes). Scale bar, 6 µm.

17

18
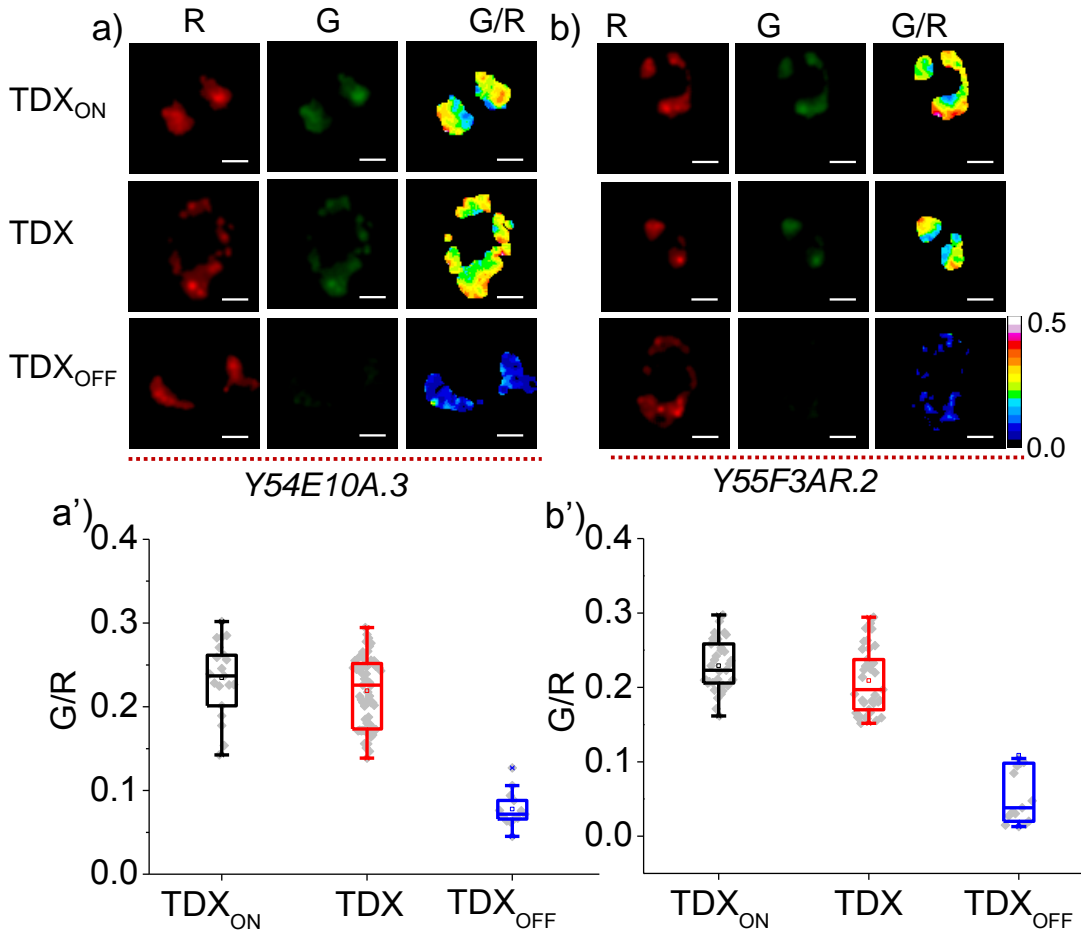
Supplementary Fig. 5. Pseudocolour images and quantification data for TDX_{ON}, (upper panel) TDX (middle panel) and TDX_{OFF} (lower panel) at 20 min time post injection (a and b) and their respective G/R ratio plot at 20 min post injection for (a' and b') for *Y54E10A.3, Y55F3AR.2* RNAi worm respectively. The RNAi of these genetic background worms have no effect on endolysosomal disulfide reduction. Scale bar, 5 μm
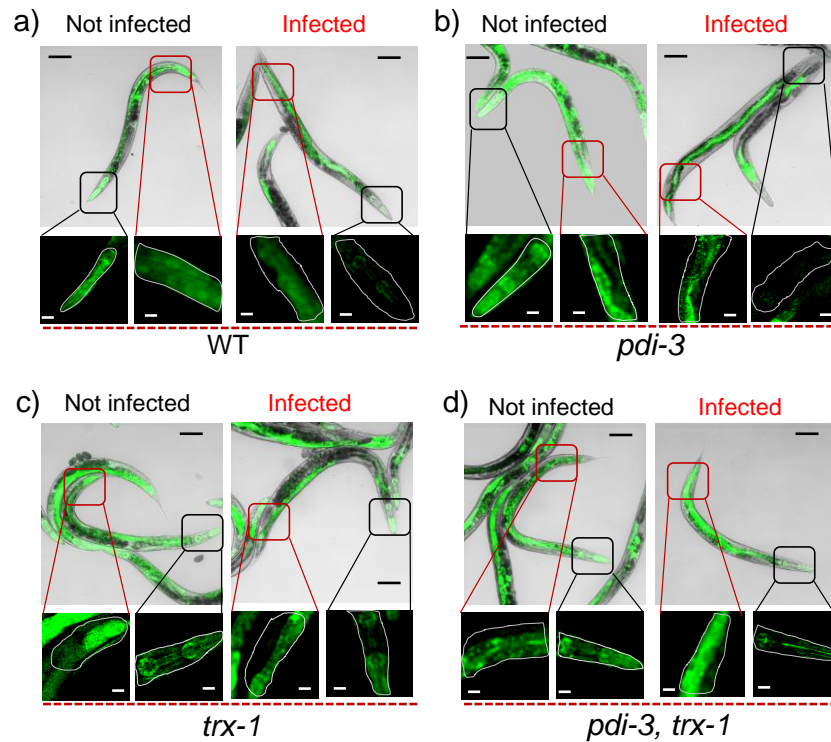
Supplementary Fig. 6. Overlay of GFP and DIC images of indicated genetic background worms with or without infection of toxic *C. diphtheria* strain. Black and red box representing pharynx and gut respectively from where the GFP intensities were taken into consideration for measurement. No of worms used in each experiment is 20. Scale bar, 100µm.

Diphtheria toxin inhibits GFP expression in pharynx

We also used another strain of the *C. diphtheriae* which produces diphtheria toxin lacking 149 amino acids at the C terminus domain of the DT-B chain. This mutation has been shown to significantly reduce uptake of the toxin by host cells by lowering the receptor binding affinity [9]. Here we observed that, *C. elegans* has identical GFP expression in pharynx and gut irrespective of infection with this strain of *C. diphtheriae.* This observation confirms that reduced GFP expression in the pharynx is caused by the toxin rather than colonization of bacteria inside the pharynx (Supplementary Fig. 7)

1
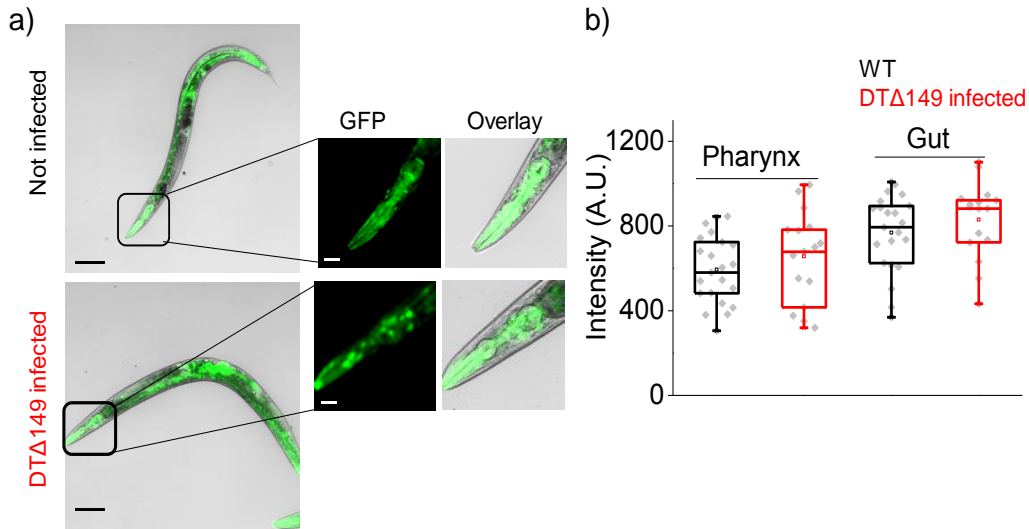
2

3 Supplementary Fig. 7. a) Overlay of GFP and DIC images of *C. elegans* with or without
4 infection of less toxic *C. diphtheria* strain (DTΔ149). The black box is showing the zoomed
5 image of pharynx which shows that GFP intensity of pharynx of DTΔ149 infected animal is
6 comparable with non-infected one. b) Plot of GFP intensity of pharynx and gut for DTΔ149
7 infected and non- infected worms. No of worms used in each experiment is 20. Scale bar,
8 100µm.
9
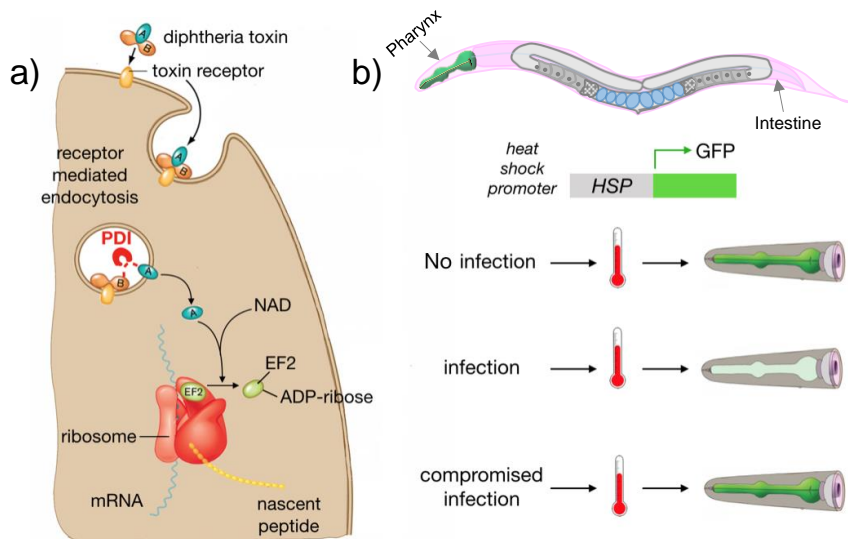
21 Supplementary Fig. 8. Diphtheria toxin infection in *C. elegans*: a) diphtheria toxin (DT) binds
22 to cell surface receptor and undergoes endocytosis. Inside the endosome the luminal acidic

pH causes a conformational rearrangement of DT. This is followed by reduction of the disulfide linker and complete translocation of the A chain to the cytosol. The A chain catalyzes the transfer of the ADP-ribose moiety of nicotinamide adenine dinucleotide (NAD+) to the diphthamide residue of the protein elongation initiation factor 2 (eEF2) inhibiting protein synthesis in the infected cell. b) A transgenic worm that express GFP in all tissues upon heat shock was used to study the effect of DT infection. Infected worms show inhibited protein synthesis which leads to reduced GFP expression in the pharynx upon heat shock. The inhibition of disulfide reduction inside the endosome compromises the mechanism of infection which leads to comparable GFP expression to the uninfected worms.
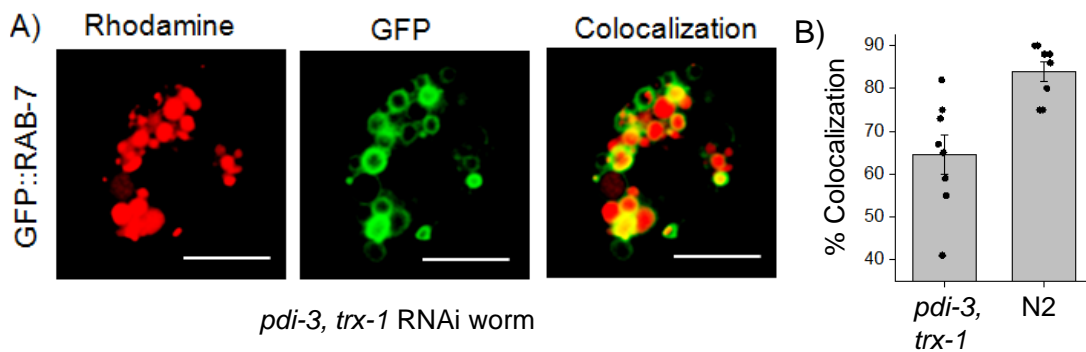
Supplementary Fig. 9. a) Colocalization of GFP::RAB-7 with TDX^R at 20 min post injection of *pdi-3, trx-1* double RNAi worm. It confirms that the endosomal trafficking is not disturbed due to knock down of these two gene by RNAi. b) Percentage (%) colocalization of TDX^R with *pdi-3, trx-1* double RNAi worm and wild type (N2) worm at 20 min post injection. (n=10 cells, ≥ 50 endosome). Scale bar, 5μm.

a)

b)

c)

Supplementary Fig.10. The chemical structure of conjugatable version of (a) Atto 647N, (b) rhodamine Red X, (c) Alexa 647

Targeting TDX reporter to endolysosomal pathway in HeLa cells:

We incubated HeLa cells with TDX reporter (1 µM) containing DMEM without FBS for 1 h at 37 °C. Cells were then washed with PBS (pH=7.4) thrice to remove any un-internalized TDX nanodevice and incubated for various chase times in DMEM complete media. Prior to imaging, cells were washed with PBS and imaged in HBSS (Hank's Balanced Salt Solution, GE healthcare) buffer. Similar protocol was followed for TDX_{ON} and TDX_{OFF} reporters.
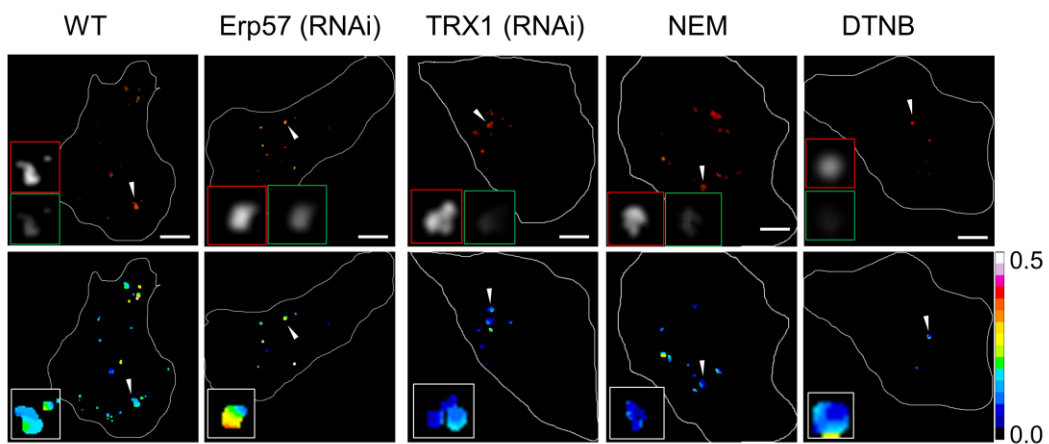
Supplementary Fig. 11: Representative pseudo-colored images (upper panel) and G/R map (lower panel) of TDX reporter pulse-chased in HeLa cells at indicated time points. Scale bar = 10 μm.

RNAi knockdown and pharmacological inhibition in HeLa cells:

All relevant siRNAs were procured from Dharmacon, Inc. HeLa cells were split on imaging dish at 1×10^4 seeding density. After 16 h in culture, the cells were transfected with siRNAs using DharmaFECT1 (Dharmacon; Catalogue No: T-2001-01) transfection reagent according to the manufacturer's protocol. For Erp57 and TRX-1 knockdown, HeLa cells were transfected with Erp57 siRNA[10] (5'-GGGCAAGGACUUACUUAUUTT-3') and TRX-1 siRNA (Dharmacon, Inc., Catalogue No: M-006340-010005). As a negative control, we used the NC siRNA (Dharmacon, Inc., Catalogue No: D-001210-01-05). After 72 h of transfection, cells were incubated with the tripartite TDX reporter for 1 h in DMEM without FBS and chased for 3 h in complete media and imaged as described earlier.

For pharmacological inhibition, cells were incubated with complete media containing either NEM (10 μM) or DTNB (100 μM) for 1 h, followed by 1 h of incubation with TDX reporter in DMEM without FBS. The cells were chased for 4 h in complete media containing either 10 μM NEM or 100 μM DTNB, washed with PBS and imaged as described in HBSS buffer containing either 10 μM NEM or 100 μM DTNB so that the relevant pharmacological inhibitor was always present.

13

Supplementary Fig. 12: Representative pseudo-color images (upper panel) and G/R map (lower panel) of TDX reporter pulse-chased to endosomes of HeLa cells, treated with indicated RNAi and inhibitors. [NEM = N ethyl maleimide, DTNB = 5,5-dithio-bis-(2-nitrobenzoic acid)]. Scale bar = 10 μm.

<u>Colocalization of TDX^{A647} with endocytic tracers</u>:

To determine where along the endolysosomal pathway the TDX reporter localized at 3 h post internalization, we performed colocalization assays with different endocytic markers. Early endosomes and late endosomes were marked by transiently transfecting HeLa cells with either Rab5-RFP or Rab7-RFP. Lysosomes were marked by pulsing TMR-dextran (1 mg/mL) for 1 h followed by 12 h chase. mRFP-Rab5 and mRFP-Rab7 was received as a gift from Ari Helenius (Addgene plasmid # 14437 and # 14436 respectively). Transfected cells were treated with DMEM (-FBS) containing TDX^{A647} (1 μM) for 15 min and then chased for 3 h in complete media and imaged in HBSS buffer. Lysosome colocalization was studied by pre-labelling HeLa cells with TMR-dextran as above and then pulsing TDX^{A647} for 15 min and chased for 3 h and imaged as described.

1
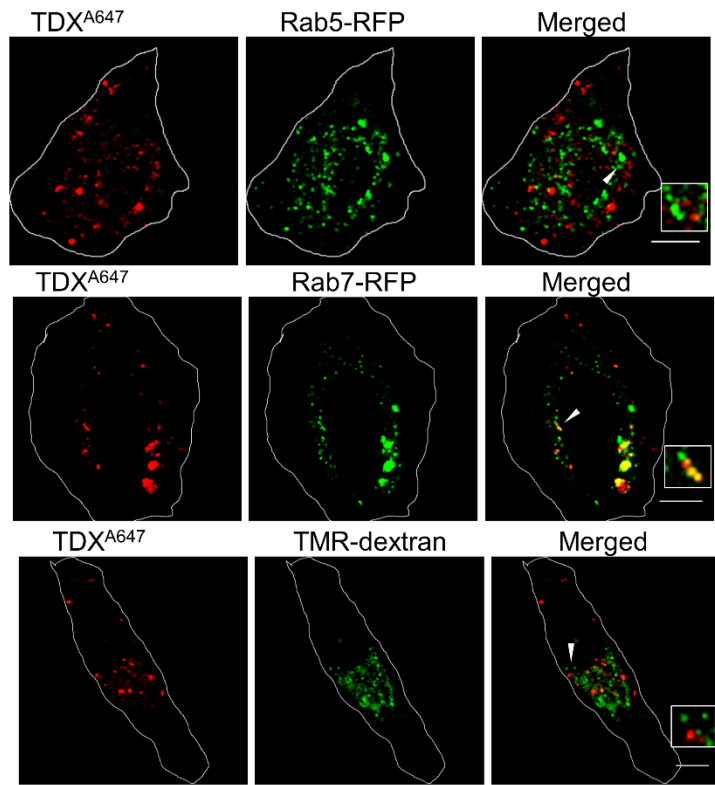
2 Supplementary Fig. 13: Representative pseudo-color images for the colocalization between

3 TDX^{A647} (red) and specific marker (green) of different endocytic vesicles after 3 h pulse chase

4 of TDX^{A647} in HeLa cells. Scale bar = 10 μm.

5

1 <u>Generalization using a new enzymatic probe</u>

2 To demonstrate the generality of our *in-situ* enzyme activity detection technology, we provide

3 data on another sensor for Cathepsin C that detects Cathepsin activity *in situ*, in lysosomes of

4 live cells. This generalizes our technology across (a) cell lines (b) organelles and (c) enzyme

5 class. Please note that the detection chemistry *per se* can be generalized to not just cathepsin

6 C, but to all the enzymes indicated in Supplementary Table S3, by simply retaining a specific

7 peptide substrate motif and swapping out *4-MU* in Table 1 for Rhodamine attached to a DNA

8 strand (Figure R2a and R2c).

9 Our platform leverages 4-methyl umbelliferone (4-MU) detection technology that is applicable

10 to a whole host of lysosomal enzymes (Supplementary Table S3). 4-MU detection technology

11 is the gold-standard in clinics, called the "enzyme test" for detecting the activity of specific

12 lysosomal enzymes, by crushing the cell and adding 4-MU to cell lysate [11].

13 We show using a DNA-based sensor that we can localize a known enzyme chemistry within

14 lysosomes inside cells and map activity of the corresponding enzyme *in situ* inside lysosomes

15 of live innate immune cells. We show this by replacing 4-MU in the 4-MU substrate for

16 Cathepsin C with a Rhodamine [12–14]. The Rhodamine fluorescence is caged by the cathepsin

17 C cleavable motif, the Gly-Phe dipeptide.

18 Cathepsins are well known lysosome-resident proteases critical role to protein or pathogen

19 degradation, amino acid recycling, bone remodeling, antigen presentation etc [15–19]. Although

20 several excellent fluorescent probes for cathepsins exist, none can detect cathepsin activity

21 exclusively in the lysosome without modifying the enzyme [16]. For example, activity based

22 probes (ABPs) are "suicide substrates", that remain attached to the enzyme in the lysosome

23 by covalent bond formation and inactivates the enzyme post-reaction with the substrates[20].

24 On the other hand, fluorogenic substrates are ideal for enzyme kinetics but the cleaved probe

25 diffuses rapidly post reaction and spatial information is rapidly lost [15].

26

1

2 Supplementary Fig. 14: A DNA-based Cathepsin C reporter: a) Sensing principle of the 4-MU
3 based substrate for the cathepsin C enzyme that cleaves the dipeptide Gly-Phe. b) A different
4 fluorescent, activity-based probe BMV109 [21], for pan Cathepsin using different fluorophore. c)
5 Structure of our Cathepsin C reporter (Cat) is a DNA duplex (black ladder), bearing a sensing
6 module (grey) and normalizing module (red). d) Sensing module is a rhodamine dye (green)
7 protected by Gly-Phe motifs and the normalizing module (orange) is Alexa647. e) Cathepsin
8 C cleaves the sensing module to uncage rhodamine fluorescence giving the highly fluorescent
9 Cat_{ON}.

10 The methodology described in the main manuscript enables us to incorporate a fluorogenic
11 substrate onto a lysosome targeted DNA device and ratiometrically map cathepsin C activity
12 while retaining stable spatial resolution at the level of the organelle.

13 The **reporter module** in the reporter "**Cat**" consists of a DNA strand (R), bearing an azido-
14 rhodamine with both amines protected by coupling to dipeptide moieties (Supplementary
15 Figure 14A-B) that are substrates for a specific cathepsin [22]. Cathepsin C cleaves the N-
16 terminus of the dipeptide Gly-Phe (Supplementary Figure 14E) [14,23]. This uncages rhodamine
17 fluorescence. The azido-Rhodamine-(Gly-Phe)$_2$ is attached to a dibenzylcyclooctyl-DNA
18 strand (DBCO-DNA) by click chemistry to give strand O_1 (Supplementary Figure 14C). The
19 **normalizing module** uses an Alexa647N labeled DNA strand, O_2 complementary to
20 O_1(Supplementary Figure 14C). The **targeting moiety** comprises the duplex O_2 O_1 which

1 localizes in lysosomes of J774A.1 cells by uptake via the scavenger receptor-mediated

2 endocytic pathway (Supplementary Figure 14C) [24–27]

3
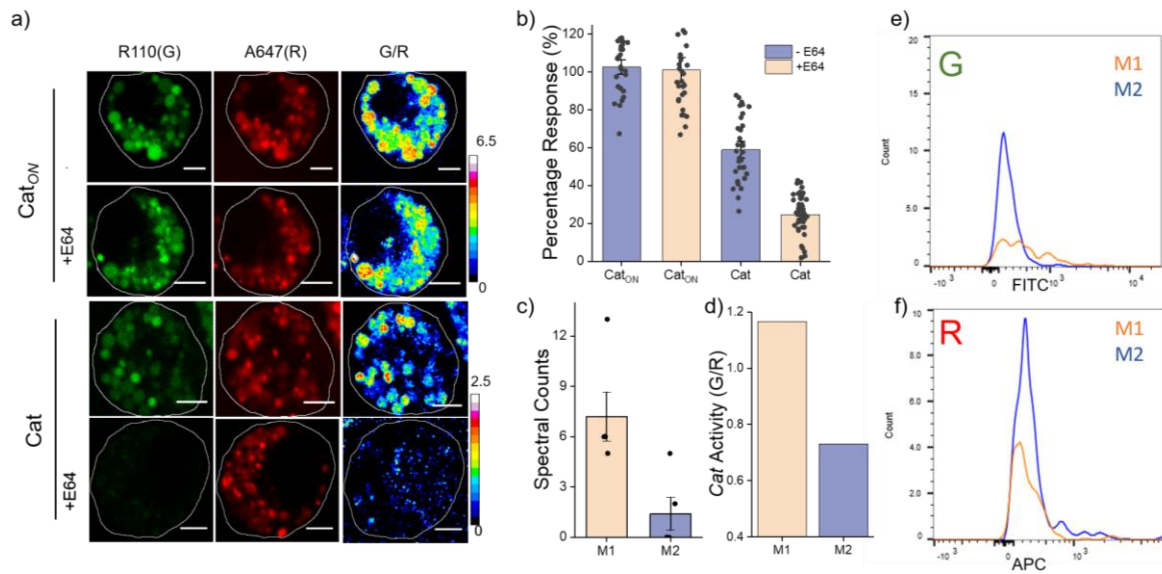
4 Supplementary Fig. 15**:** Mapping cathepsin C activity in lysosomes of live cells**.** a)

5 Representative pseudo-color images of lysosomally localized **Cat** probes in J774A.1 cells, b)

6 Box plot showing G/R ratio of reporters in the presence and absence of 200 µM E64 (n = 50

7 cells, ≥ 150 endosome). Scale bar, 5 µm. c) Cathepsin C levels by proteomics in primary bone

8 marrow derived murine M1 and M2 macrophages (BMDMs) d) Cathepsin C activity as

9 revealed by G/R ratio of M1 and M2 BMDMs with the **Cat** probe using flow cytometry (e,f) on

10 ~10^5 cells.

11

12 We incubated the cells - with or without Cathepsin inhibitor E64 - and 500 nM of either **Cat** or

13 **Cat$_{ON}$** probes separately for 30 min at 37° C. After 1 h, cells were washed and imaged live in

14 the Rhod (G, λem = 520 nm) and Alexa 647 (R, λem = 670 nm) channels. The **Cat$_{ON}$** probe

15 provides the maximum possible ratiometric signal G/R (Rhodamine/Alexa647N) if the **Cat**

16 probes was cleaved to its fullest extent. All G/R values were normalized to that of **Cat$_{ON}$**.

17 The G/R maps clearly revealed maps of high cathepsin C activity in lysosomes, which in the

18 presence of the cathepsin inhibitor E64, showed maps of low cathepsin C activity and low G/R

19 ratios (Supplementary Figure 15A-B) [28]. This was borne out even in bone-marrow-derived

20 primary macrophages from mice that have been activated (M1-like, high cathepsin C activity)

21 and non-activated (M2-like, low cathepsin C activity) (Supplementary Figure 15C-D).

22 Proteomics reveals that M1-like macrophages have high cathepsin C levels and M2-like

23 macrophages have low cathepsin C levels. The intensity values in the G (Supplementary

24 Figure 15E) and R channels (Supplementary Figure 15F) for ~10^5 cells passed through a flow-

25 cytometer are shown. Despite M2 macrophages uptaking more probe (higher values, blue

trace) than the M1 macrophages, these show lower cathepsin C activity (lower G/R intensity ratio, Supplementary Figure 15D) consistent with the proteomics data (Supplementary Figure 14C). Supplementary Figure 15A shows sub-cellular information and therefore magnified to show the information for a single/two cells.

Supplementary Table 1: Azido and Rhodamine labelled oligonucleotide sequences used for TDX reporters and others are used as primers for RT-PCR experiment.

Name	Sequence	Comment
O-Azide	5'-<u>Azide</u>-AT ATA TAT GCC GAC TGC TGC ACT GAC CGC AGG AT-3'	Azide labelled DNA strand
O-Rhodamine Red X	5'-<u>RhoR</u>-AT CCT GCG GTC AGT GCA GCA GTC GGC ATA TAT AT-3'	Rhodamine Red X labelled DNA strand
O1F	5'-AATTCGGAGTTAAGGGATTC-3'	Forward Primer RT-PCR *pdi-3* gene
O1R	5'-TTGGTCCATTGGATACTTTC-3'	Reverse Primer RT-PCR *pdi-3* gene
O2F	5'-GAAGCCGCGAAAAGAGAGTA-3'	Forward Primer RT-PCR *C30H7.2* gene
O2R	5'-AAGCAGGCTTCAACTTCTCG-3'	Reverse Primer RT-PCR *C30H7.2* gene
O3F	5'-CTTCAAAAATGACACAATTACG-3'	Forward Primer RT-PCR *trx-2* gene
O3R	5'-GAGAACGTCCTCGATAAAATC-3'	Reverse Primer RT-PCR *trx-2* gene
O4F	5'-CTTGCTGATATGAGTGACTTTG-3'	Forward Primer RT-PCR *trx-1* gene
O4R	5'-ATACGTGCTCCAACACTTTTT-3'	Reverse Primer RT-PCR *trx-1* gene

1   Supplementary Table 2: Thioredoxin domain containing proteins present in *C. elegans*
2   obtained from BLASTP search against *C. elegans* genome. Corresponding e values from best
3   BLASTP match with *H. Sapiens* genome.

|	Candidate protein	E value
C elegans protein containing thioredoxin domain	PDI-1	9.59 e-108
	PDI-2	5.3 e-155
	PDI-6	1.4 e-131
	C14B9.2	4.1e-155
	PDI-3	4.3 e-112
	Y49E10.4	7.4e-101
	M04D5.1	5.8e-29
	C30H7.2	1.4e-90
	TRX-1	8.9e-18
	TRX-2	1.1e-261
	Y73B6BL.12	1.3e-17
	Y55F3AR.2	9.9e-19
	Y54E10A.3	8.2e-63
	dpy-11	2.5e-54
	C35D10.10	8.1e-50
	F56G4.5	8.7e-75
Thioredoxin protein with mitochondrial localization signal	F35G2.1	1.5e-43
	T10H10.2	7.8e-49
	F47B7.2	3.3e-57
Thioredoxin protein with nuclear localization signal	C35B1.5	1.1e-19
	trx-5	4e-22
	trx-3	5e-15
	F29B9.59	3e-17

4

1 Supplementary Table 3: A selection of 4-methyl umbelliferone (4-MU) based substrate probes

2 that are used as diagnostics for genetic lysosomal diseases that are due to deficient activity

3 of the indicated lysosome-resident enzymes. **FDA-approved diagnostics based on the 4-MU

4 substrate cleavage assay.

Lysosomal Enzyme	*4-MU*-based Substrate probe	Lysosomal Disease	Reference
Cathepsin C (CTSC)	H-Gly-Phe-*4-MU*	Papillon–Lefèvre syndrome	2914
Cathepsin D (CTSD)	*4-MU*-Gly-Lys-Pro-Ile-Leu-Phe-Phe-Arg-Leu-Lys(Dnp)-D-Arg-NH2	Congenital neuronal ceroid-lipofuscinosis	30,31
α-Galactosidase A (GLA)	*4-MU*-α-galactoside	Fabry Disease	3233**
Acid β-glucosidase (GBA)	*4-MU*-β-D-glucoside	Gaucher Disease	34**
β-Galactocerebrosidase (GALC)	6-Hexadecanoylamino-*4-MU* -β-D-galactoside	Krabbe Disease	35
α-L-iduronidase (IDUA)	*4-MU*-α-L-iduronide	MPS-I (Hurler, Hurler-Scheie and Scheie syndrome)	36,37
Iduronate-2-sulfatase (IDS)	*4-MU*-1-iduronide-2-sulphate	MPS-II (Hunter syndrome)	38
N-acetyl-galactosamine-6-sulfatase (GALNS)	*4-MU*-β-D-galactoside-6-sulphate	MPS-IVA (Morquiosyndrome, type A)	39
Acid sphingomyelinase (ASM)	6-Hexadecanoylamino-*4-MU*-phosphorylcholine	Niemann-Pick Disease, type A and B	40
Acid α-glucosidase (GAA)	*4-MU*-α-D-glucoside	Pompe Disease (Glycogen Storage Disease, type II)	41**

5

A)

B)
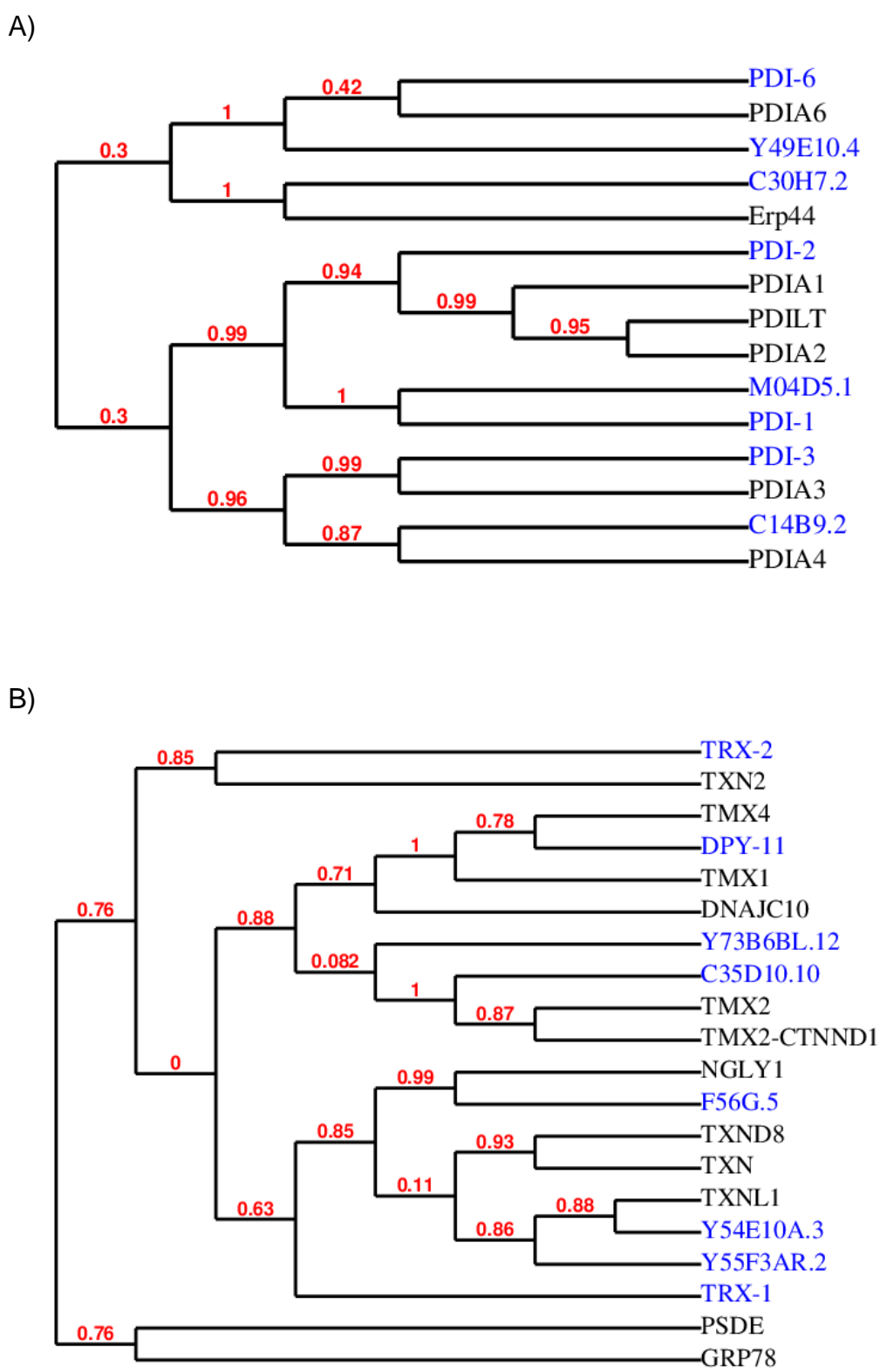
Supplementary Fig. 16: Phylogenetic tree comparing the proteins having a) more than one thioredoxin domain (upper) and b) one thioredoxin domain (lower) of *C. elegans* (blue) with *H. sapiens* (black). The numbers, in red, next to each node represent a measure of sequence similarity for the node. These are generally numbers between 0 and 1 where 1 represents maximal similarity.

References:

1. Molla, M. R. & Ghosh, S. Exploring versatile sulfhydryl chemistry in the chain end of a synthetic polylactide. *Macromolecules* **45,** 8561–8570 (2012).

2. Mugherli, L., Burchak, O. N., Chatelain, F. & Balakirev, M. Y. Fluorogenic ester substrates to assess proteolytic activity. *Bioorg Med Chem Lett* **16,** 4488–4491 (2006).

3. Dubikovskaya, E. A., Thorne, S. H., Pillow, T. H., Contag, C. H. & Wender, P. A. Overcoming multidrug resistance of small-molecule therapeutics through conjugation with releasable octaarginine transporters. *Proc Natl Acad Sci U S A* **105,** 12128–12133 (2008).

4. Lloyd, J. B. Disulphide reduction in lysosomes. The role of cysteine. *Biochem J* **237,** 271–272 (1986).

5. Wu, Z., Liang, D. & Tang, X. Visualizing Hydrogen Sulfide in Mitochondria and Lysosome of Living Cells and in Tumors of Living Mice with Positively Charged Fluorescent Chemosensors. *Anal Chem* **88,** 9213–9218 (2016).

6. Yang, J., Chen, H., Vlahov, I. R., Cheng, J.-X. & Low, P. S. Evaluation of disulfide reduction during receptor-mediated endocytosis by using FRET imaging. *Proc Natl Acad Sci U S A* **103,** 13872–13877 (2006).

7. FeenerS, E., Shene, W.-C. & Ryser, H. Cleavage of Disulfide Bonds in Endocytosed Macromolecules.

8. Bhatia, D. *et al.* Icosahedral DNA nanocapsules by modular assembly. *Angew Chem Int Ed Engl* **48,** 4134–4137 (2009).

9. Pappenheimer, A. M. Diphtheria toxin. *Annu Rev Biochem* **46,** 69–94 (1977).

10. Xu, D., Perez, R. E., Rezaiekhaligh, M. H., Bourdi, M. & Truog, W. E. Knockdown of ERp57 increases BiP/GRP78 induction and protects against hyperoxia and tunicamycin-induced apoptosis. *Am J Physiol Lung Cell Mol Physiol* **297,** L44–51 (2009).

11. Yu, C., Sun, Q. & Zhou, H. Enzymatic screening and diagnosis of lysosomal storage diseases. *N Am J Med Sci (Boston)* **6,** 186–193 (2013).

12. Li, J. *et al.* Substrate optimization for monitoring cathepsin C activity in live cells. *Bioorg Med Chem* **17,** 1064–1070 (2009).

13. Leytus, S. P., Melhado, L. L. & Mangel, W. F. Rhodamine-based compounds as fluorogenic substrates for serine proteinases. *Biochem J* **209,** 299–307 (1983).

14. McGuire, M. J., Lipsky, P. E. & Thiele, D. L. Purification and characterization of dipeptidyl peptidase I from human spleen. *Arch Biochem Biophys* **295,** 280–288 (1992).

15. Turk, V. *et al.* Cysteine cathepsins: from structure, function and regulation to new frontiers. *Biochim Biophys Acta* **1824,** 68–88 (2012).

16. Vasiljeva, O. *et al.* Emerging roles of cysteine cathepsins in disease and their potential as drug targets. *Curr Pharm Des* **13,** 387–403 (2007).

17. Berdowska, I. Cysteine proteases as disease markers. *Clin Chim Acta* **342,** 41–69 (2004).

18. Jedeszko, C. & Sloane, B. F. Cysteine cathepsins in human cancer. *Biol Chem* **385,** 1017–1027 (2004).

19. Guha, S. & Padh, H. Cathepsins: fundamental effectors of endolysosomal proteolysis. *Indian J Biochem Biophys* **45,** 75–90 (2008).

20. Watzke, A. *et al.* Selective activity-based probes for cysteine cathepsins. *Angew Chem Int Ed Engl* **47,** 406–409 (2008).

21. Edgington-Mitchell, L. E., Bogyo, M. & Verdoes, M. Live Cell Imaging and Profiling of Cysteine Cathepsin Activity Using a Quenched Activity-Based Probe. *Methods Mol Biol* **1491,** 145–159 (2017).

22. Leytus, S. P., Patterson, W. L. & Mangel, W. F. New class of sensitive and selective fluorogenic substrates for serine proteinases. Amino acid and dipeptide derivatives of rhodamine. *Biochem J* **215,** 253–260 (1983).

23. Berg, T. O., Strømhaug, E., Løvdal, T., Seglen, O. & Berg, T. Use of glycyl-L-phenylalanine 2-naphthylamide, a lysosome-disrupting cathepsin C substrate, to distinguish between lysosomes and prelysosomal endocytic vacuoles. *Biochem J* **300 (Pt 1),** 229–236 (1994).

24. Modi, S., Nizak, C., Surana, S., Halder, S. & Krishnan, Y. Two DNA nanomachines map pH changes along intersecting endocytic pathways inside the same cell. *Nat Nanotechnol* **8,** 459–467 (2013).

25. Modi, S. *et al.* A DNA nanomachine that maps spatial and temporal pH changes inside living cells. *Nat Nanotechnol* **4,** 325–330 (2009).

26. Saha, S., Prakash, V., Halder, S., Chakraborty, K. & Krishnan, Y. A pH-independent DNA nanodevice for quantifying chloride transport in organelles of living cells. *Nat Nanotechnol* **10,** 645–651 (2015).

27. Chakraborty, K., Leung, K. & Krishnan, Y. High lumenal chloride in the lysosome is critical for lysosome function. *elife* **6,** e28862 (2017).

28. Barrett, A. J. *et al.* L-trans-Epoxysuccinyl-leucylamido(4-guanidino)butane (E-64) and its analogues as inhibitors of cysteine proteinases including cathepsins B, H and L. *Biochem J* **201,** 189–198 (1982).

29. Hamon, Y. *et al.* Analysis of urinary cathepsin C for diagnosing Papillon-Lefèvre syndrome. *FEBS J* **283,** 498–509 (2016).

30. Yasuda, Y. *et al.* Characterization of new fluorogenic substrates for the rapid and sensitive assay of cathepsin E and cathepsin D. *J Biochem* **125,** 1137–1143 (1999).

31. Persichetti, E. *et al.* Factors influencing the measurement of lysosomal enzymes activity in human cerebrospinal fluid. *PLoS ONE* **9,** e101453 (2014).

32. Fabry Disease Enzyme Analysis (alpha... | Integrated Genetics. at <https://www.integratedgenetics.com/test-menu/39311/fabry-disease-enzyme-analysis-alpha-galactosidase-a>

33. Nakanishi, T., Funahashi, S., Funai, T., Hashimoto, T. & Shimizu, A. Chemical diagnosis of Fabry's disease by fluorometric assay and fast atom bombardment/mass spectrometry. *Ann Clin Biochem* **28 (Pt 4),** 368–372 (1991).

34. Robinson, D. The fluorimetric determination of beta-glucosidase:' ' its occurrence in the tissues of animals, including insects. *Biochem J* **63,** 39–44 (1956).

35. Wiederschain, G., Raghavan, S. & Kolodny, E. Characterization of 6-hexadecanoylamino-4-methylumbelliferyl-beta-D- galactopyranoside as fluorogenic substrate of galactocerebrosidase for the diagnosis of Krabbe disease. *Clin Chim Acta* **205,** 87–96 (1992).

36. He, W., Voznyi YaV, Boer, A. M., Kleijer, W. J. & van Diggelen, O. P. A fluorimetric enzyme assay for the diagnosis of Sanfilippo disease type D (MPS IIID). *J Inherit Metab Dis* **16,** 935–941 (1993).

37. Voznyi YaV *et al.* A fluorimetric enzyme assay for the diagnosis of Sanfilippo disease C (MPS III C). *J Inherit Metab Dis* **16,** 465–472 (1993).

38. Voznyi, Y. V., Keulemans, J. L. & van Diggelen, O. P. A fluorimetric enzyme assay for the diagnosis of MPS II (Hunter disease). *J Inherit Metab Dis* **24,** 675–680 (2001).

39. Wood, T. C. *et al.* Diagnosing mucopolysaccharidosis IVA. *J Inherit Metab Dis* **36,** 293–307 (2013).

40. Van Diggelen, O. P. *et al.* A new fluorimetric enzyme assay for the diagnosis of Niemann-Pick A/B, with specificity of natural sphingomyelinase substrate. *J Inherit Metab Dis* **28,** 733–741 (2005).

41. Butterworth, J. & Droadhead, D. M. Diagnosis of Pompe's disease in cultured skin fibroblasts and primary amniotic fluid cells using 4-methylumbelliferyl-alpha-D-glucopyranoside as substrate. *Clin Chim Acta* **78,** 335–342 (1977).